PROCESS-BASED MODELING OF THE OVERFLOW-INDUCED GROWTH OF EROSIONAL CHANNELS

THIEU QUANG TUAN

Faculty of Coastal Engineering

Water Resources University (WRU)

175 Tay Son, Dong Da District, Hanoi, Vietnam

Corresponding author, email: Tuan.T.Q@wru.edu.vn, phone: +84.4.5634415, *fax:* +84.4.5635832

MARCEL J.F. STIVE[+], HENK JAN VERHAGEN[++], and PAUL J. VISSER[+++]

Section of Hydraulic Engineering

Faculty of Civil Engineering and Geosciences

Delft University of Technology (DUT)

Stevinweg 1, P.O. Box 5048, 2600 GA Delft, the Netherlands.

[+] *M.J.F.Stive@tudelft.nl*

[++] *H.J.Verhagen@tudelft.nl*

[+++] *P.J.Visser@tudelft.nl*

Abstract

A new process-based approach is introduced for a more efficient computation of the overflow-induced growth of an erosional channel in a non-cohesive homogeneous narrow landmass such as the breach growth in a sand-dike. The approach is easy to incorporate in a 1D/2DV morphodynamic model to compute the channel growth both vertically and laterally.

The flow modeling is based on the shallow water equations. For modeling the channel growth, a set of closed equations describing the channel growth in both vertical and lateral direction has been derived in connection with several new morphologic parameters such as the representative channel width and the channel cross-sectional growth index.

The approach has been applied to simulate the breach growth in sand-dikes and the morphological development of wave overwash across sand barriers. The computational results bear fairly good resemblance with existing experimental data.

Keywords: Overwash, Breach growth modeling, Wave overtopping, Breach widening, Breach deepening, Breach growth index, Sand dikes, Coastal barriers.

1 Introduction

Morphological development of an erosional channel induced by ‘flash’ overflow is commonly encountered in hydraulic engineering applications. Typical practical situations are the morphological development of a breach in a narrow landmass (breach growth in a dike or barrier) due to overflow and that of an overwash channel in a coastal barrier due to wave overtopping. It is of practical interest to quantify this process of development both vertically and laterally. However, three-dimensional morphodynamic modeling of this phenomenal process requires lots of efforts and is computationally expensive. Therefore, it is preferable to use approaches which are more efficient (simpler but sufficiently reliable) for some specific applications such as uses of parametric or analytical approaches for modeling of breach growth in sand dikes (see e.g. Visser, 1998; Kraus, 2003). In these approaches, assumptions about the channel morphological evolution, e.g. evolutional stages or growth toward equilibrium, must be imposed and therefore they are valid within their application limits only. For more generic applications a process-based approach is needed, however, with more modeling challenges. In the following we address some of these challenges that lead to implications on a new approach to resolve the considered problem.

Regarding the flow characteristics, the flow in an overflow situation is unsteady and displays discontinuities such as intermittences (overwash flow) and hydraulic jumps (breach flow). Also, it can be in the mixed-regime (breach flow) and can be very shallow (overwash flow). Abrupt and arbitrary variations of the channel bed, especially in the case of breaching, further bring about difficulties to the modeling of this flow. All these aspects require a robust numerical method such as an upwind approach in order to capture such complex flow conditions reliably.

Concerning channel morphology, the channel growth is a result of an erosion process induced by the flow. By the nature of the process, bed changes are much more dynamic in the streamwise direction than those in the transverse direction. Also, the channel length in the case of breaching and overwash is relatively short (the channel through a narrow landmass), so the streamwise variation of the channel width is negligible compared to the streamwise variation of the channel bed. As a result, the bed profile along the channel (the vertical growth) must be known in detail while an instantaneous uniform width quantity is usually sufficient to represent the overall channel lateral growth. Moreover, the existence of a morphological relation between the lateral and the vertical growths of an erosional channel in a non-cohesive homogeneous landmass has been implicated by various researchers such as Visser (1998), Busnelli (2001) and Kraus (2003) in their studies on the breach growth. However, as discussed in Subsection 3.1, no relation has been found that describes the nature of the process of the channel growth appropriately.

From the above arguments, it is feasible to develop an approach for a more efficient computation of the morphological development of erosional channels, in which the channel growth in lateral direction is quantified in relation to that in vertical direction. For the sake of simplicity, this approach is designated as the MOGEC approach hereinafter (Modeling of Overflow-induced Growth of Erosional Channels).

In Section 2 we briefly introduce a selected upwind numerical method to resolve the general equations for open channel flows. An approach for treatment of source terms arising from friction and bed variation is also described. Modeling of the channel growth using a new process-based approach is discussed in Section 3. Applications of the developed approach for simulating breach growth and overwash development are given in Section 4. The paper ends with a summary and conclusions drawn in Section 5.

2 Flow modeling

2.1 Basic flow equations

One-dimensional unsteady flow of water in a channel of slowly varying cross-section is governed by the Saint Venant equations. For flows in prismatic channels of arbitrary cross-section, the equations in conservative form read:

$$\frac{\partial U}{\partial t}+\frac{\partial F(x,U)}{\partial x}=S(x,U) \tag{1}$$

with conserved vectors U, $F(x,U)$, and source term vector $S(x,U)$ arising from bed slope and friction are as follows:

$$\begin{aligned} U(x)&=\begin{pmatrix} A \\ Q \end{pmatrix} \\ F(x,U)&=\begin{pmatrix} Q \\ \frac{Q^2}{A}+gI_P \end{pmatrix} \\ S(x,U)&=\begin{pmatrix} 0 \\ gA(S_{bx}-S_f) \end{pmatrix} \end{aligned} \tag{2}$$

in which A is the wetted cross-sectional area, Q is the discharge, S_{bx} and S_f are bed slope and friction slope, respectively, I_P is a hydrostatic pressure force term acting on the wetted area.

$$\begin{aligned} S_f&=\frac{1}{C^2}\frac{Q^2}{A^2R} \\ I_P&=\int_0^d (d-z)B(z)dz \\ S_{bx}&=-\frac{dZ_b}{dx} \end{aligned} \tag{3}$$

where C is the Chezy coefficient, R is the hydraulic radius, and $B(z)$ is channel breadth at elevation z above the bottom.

In trapezoidal channels of constant bottom width b, *IP* is further specified as:

$$I_P=\frac{1}{2}bd^2+\frac{1}{3}md^3 \tag{4}$$

Discretization of Eq. (1) using the Finite Volume Method (FVM) yields:

$$U^{n+1}=U^n-\frac{\Delta t}{\Delta x}(F_{i+1/2}-F_{i-1/2})+\Delta tS^n \tag{5}$$

in which n is a known computed level, Δt and Δx are time and space steps, respectively, $F_{i-1/2}$ and $F_{i+1/2}$ are numerical fluxes at the boundaries of a computed cell.

It is noted that by the nature of the FVM the discretization of Eq. (4) into Eq. (5) is totally exact without any approximation (see Toro, 1997).

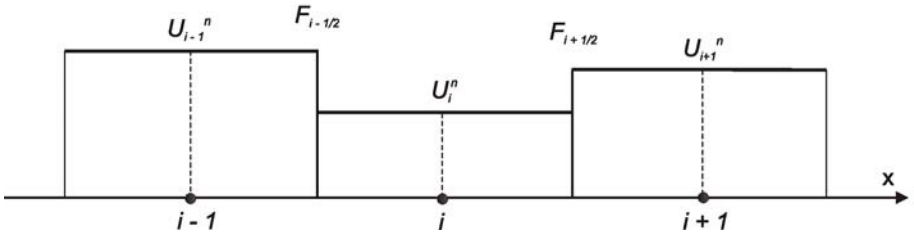

Figure 1 Boundary cell numerical fluxes and the Riemann problem

$F_{i-1/2}$ and $F_{i+1/2}$ are determined using the Riemann problem (see Fig. 1):

$$F_{i+1/2} = F_{i+1/2}(U_L, U_R) \text{ with } U = \begin{cases} U_L = U_i^n & x < x_{i+1/2} \\ U_R = U_{i+1}^n & x > x_{i+1/2} \end{cases} \tag{6}$$

2.2 Roe Riemann approximate solver

To solve Eq. (5) with the Riemann problem given by Eq. (6) and the source terms as described in Eq. (3), a robust numerical scheme must be adopted. Fortunately, recent developments in upwind schemes solved in conjunction with FVM, which were originally introduced in gas dynamics, have provided great means to overcome such difficulties. Numerical schemes of these types are conservative and therefore able to deal with the presence of discontinuities. Also, an exact solution to Eq. (6) is usually impractical and thus any appropriate approximate Riemann solver is favorable. Without loss of generality, the first-order Roe's approximation is adopted here to determine the boundary numerical fluxes. The Roe's (Roe, 1981) approximate Riemann solver has been very successful in resolving many problems of shallow water flows. Basic formulations of this approach are summarized in the following. More details of the elaboration can be found in Toro (1997).

$$F_{i\pm1/2} = \frac{1}{2}(F_i + F_{i\pm1}) - \frac{1}{2}\sum_{k=1}^{2} \alpha_{i\pm1/2}^k \mid \hat{\lambda}_{i\pm1/2}^k \mid \hat{R}_{i\pm1/2}^k \tag{7}$$

where the Roe's coefficients are:

$$\alpha_{i+1/2}^{1,2} = \frac{\Delta Q_{i+1/2} \mp \hat{\lambda}_{i+1/2}^{1,2} \Delta A_{i+1/2}}{2\hat{c}_{i+1/2}} \tag{8}$$

with $\Delta(\bullet)_{i+1/2} = (\bullet)_{i+1} - (\bullet)_i$

the eigenvalues of the Roe's matrix:

$$\hat{\lambda}_{i+1/2}^{1,2} = \hat{u}_{i+1/2} \pm \hat{c}_{i+1/2} \tag{9}$$

$$\hat{u}_{i+1/2} = \frac{Q_{i+1}/\sqrt{A_{i+1}} + Q_i/\sqrt{A_i}}{\sqrt{A_{i+1}} + \sqrt{A_i}}$$

$$\hat{c}^2_{i+1/2} = \begin{cases} g\dfrac{I_{Pi+1} - I_{Pi}}{A_{i+1} - A_i} & \text{if } A_{i+1} \neq A_i \\ \dfrac{g}{2}\left(\dfrac{A_i}{B_i} + \dfrac{A_{i+1}}{B_{i+1}}\right) = g\dfrac{A_i}{B_i} & \text{if } A_{i+1} = A_i;\ \dfrac{I_{Pi+1} - I_{Pi}}{A_{i+1} - A_i} < 0 \end{cases} \tag{10}$$

and the eigenvectors:

$$\hat{R}^{1,2}_{i+1/2} = \begin{pmatrix} 1 \\ \hat{\lambda}^{1,2}_{i+1/2} \end{pmatrix} \tag{11}$$

To be consistent with Eq. (7), the source terms in Eq. (3) have to be discretized also in such a way that the conservation properties of the scheme are well satisfied. In Garcia-Navarro and Vazquez-Cendon (2000) it is shown that this can be best achieved by up-winding also the source terms. Eq. (5) now becomes:

$$U^{n+1} = U^n - \frac{\Delta t}{\Delta x}(F_{i+1/2} - F_{i-1/2}) + \frac{\Delta t}{\Delta x}[\frac{1}{2}(\psi_L)_{i-1/2} + \frac{1}{2}(\psi_R)_{i+1/2}] \tag{12}$$

$$\psi_L = \hat{\beta}\begin{pmatrix} s_1 - s_2 \\ \hat{\lambda}^1(1+s_1) - \hat{\lambda}^2(1+s_2) \end{pmatrix} \quad \psi_R = \hat{\beta}\begin{pmatrix} s_2 - s_1 \\ \hat{\lambda}^1(1-s_1) - \hat{\lambda}^2(1-s_2) \end{pmatrix} \tag{13}$$

with $s_k = sign(\hat{\lambda}^k)$ and $\hat{\beta}$ is a discretized source term coefficient.

$$\hat{\beta} = \frac{g\Delta x}{2\hat{c}}\overline{A}(\overline{S}_{bx} - \overline{S}_f) \tag{14}$$

in which $\overline{A}$, $\overline{S}_{bx}$, and $\overline{S}_f$ are the Roe averages at a computed cell.

It is worth mentioning that extra source terms in the source term vector $S(x, U)$ in Eq. (2) might be needed to account for additional effects in some particular situations, e.g. to account for turbulence effects of a hydraulic jump in the case of the breach flow (see Subsection 4.1 and also Tuan *et al.*, 2006b). Consequently, the coefficient $\hat{\beta}$ in Eq. (14) is also modified. Source terms by infiltration through the bed are neglected even in the case of wave overwash as it is assumed that prior natural processes such as rain, seepage and capillary effects due to a high water level, etc. have caused the channel bed to be saturated.

Equation (12) is solved in time to describe the flow conditions. For this, the boundary conditions on both sides of the channel need to be specified. In principle, for the present situation, one condition, viz. time series of either the water level or the discharge, one at the upstream boundary and one at the downstream boundary are sufficient. In both cases of breaching and overwash, it is most practical to impose the time-varying water level at those boundaries. In the case of wave overwash the upstream boundary water level is given by the overtopping level as output from the wave modeling. At a computational time step the channel cross-section is characterized by a representative width as specified in Subsection 3.2

As argued by Garcia-Navarro and Vazquez-Cendon (2000), the numerical scheme discussed so far is robust, satisfying the requirement posed earlier for the flow modeling. Because the scheme is explicit, its stability is conditional according to:

$$CFL = \frac{\Delta t \lambda_{\max}}{\Delta x} < 1.0 \tag{15}$$

where CFL is the Courant number, $\lambda_{\max}$ is the maximum propagation speed of shock waves.

3 Growth of an erosional channel

3.1 Preceding studies on the breach lateral growth

Various breach models have used different methods to determine the increase of the breach width, in which a relationship between the lateral erosion and the vertical erosion of the breach is established.

In breach growth in sand-dikes by Visser (1998) the lateral growth rate in the third and fourth (unobstructed base) stages is increased linearly relative to the vertical growth rate as described in Eq. (16). The relation is in fact based on a simple geometrical argument of the trapezoidal breach cross-section, assuming that breach deepening widens the breach:

$$\frac{dB_t}{dt} = -\frac{2}{\tan\gamma_1}\frac{dZ_b}{dt} \tag{16}$$

where Z_b is the level of the breach bottom that also controls the flow rate through the breach, Bt is the top width, γ_1 is the critical angle of the side slopes.

Kraus (2003) derived an analytical model of coastal barrier breaching, in which an idealized rectangular channel cross-section is presumed and the breach evolves exponentially decaying from initial width and depth towards an equilibrium state:

$$\frac{dB}{dt} = \frac{\alpha}{h}\left(1 - \frac{B}{B_e}\right) \qquad \text{with } \alpha = \frac{Q_{s,\max}}{L} \tag{17}$$

$$\frac{dh}{dt} = \frac{\beta}{B}\left(1 - \frac{h}{h_e}\right) \qquad \text{with } \beta = \frac{Q_{b,\max}}{L} \tag{18}$$

where B and h are width and depth of the breach channel, respectively. Notations with subscript $(_e)$ correspond to equilibrium values. $Q_{s,\max}$ and $Q_{b,\max}$ are constant maximum transport rates along the sides and the bottom of the breach, respectively. L is the length of the breach.

In conclusion, the above relations are either too simplistic (only based on a geometric factor such as Eq. (16)) or only qualitative (the equilibrium breach dimensions and the maximum net transport rates along the breach need to be known in advance, i.e. Eqs. (17) and (18)) and are unsuitable for use in a process-based hydrodynamic model of breach growth. Moreover, the use of a breach width and a breach depth at a single specific location, e.g. at the middle of the breach, or assuming a constant width and a constant depth along the breach in the computation of breach growth is unrealistic.

In the following we present a new approach for modeling the morphological development of erosional channels (MOGEC) which overcomes the aforementioned drawbacks. The approach is process-based and can easily be incorporated in a morphodynamic numerical model.

3.2 General equations for channel growth and volumetric channel width

Let us consider a channel (breach or overwash channel) through a homogeneous sand barrier. The channel has an instantaneous length *L* and an instantaneous trapezoidal cross-section at an arbitrary horizontal distance *x* as described in Fig. 2.

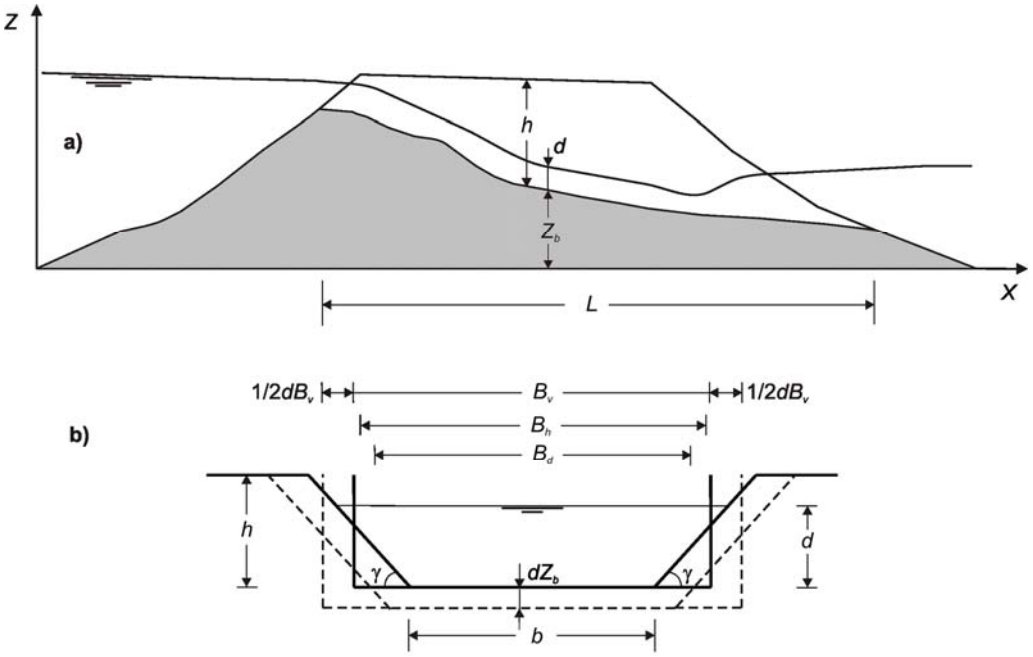

Figure 2 Definition sketch for an erosional channel in an overflow situation
a) channel longitudinal section b) arbitrary trapezoidal cross-section

Bed level changes induced by currents are modeled by solving the conventional equation of mass conservation, in which space-and-time-varying sediment transport rates have to be known. When flow is confined in a channel with also erodible banks then changes in bed level and width must both appear in the bottom elevation equation as follows:

$$\frac{\partial Z_b}{\partial t} B_h - \frac{\partial B_h}{\partial t} h + \frac{1}{(1-p)} \frac{\partial (q_s B_d)}{\partial x} = 0 \tag{19}$$

with:

$$B_h = b + \frac{h}{\tan \gamma} \qquad B_d = b + \frac{d}{\tan \gamma} \tag{20}$$

in which *Zb* is the channel bed level above a datum (see Fig. 2a), q_s is the instantaneous sediment transport rate through a unit width of the channel at the considered section, *p* is bed porosity, B_h and B_d are the depth-averaged widths over the channel depth (*h*) and water depth (*d*), respectively, *b* is the bottom width, γ is the side slope (see Fig. 2b).

It is noted that B_h, B_d, and b are the local channel widths at an arbitrary distance x. These widths are not constant and vary correspondingly to the variations of the bottom and the water depth along the channel. Hence, Eq. (19) is just a point-wise (local) equation and does not show the morphological development of the channel as a whole, particularly the increase in the channel width. However, in order to allow for a comparison with measurements we need to express the lateral growth through a nominal width, representing the channel as a whole.

For this purpose, Eq. (19) is rewritten in the following form:

$$-\frac{\partial}{\partial t}(B_h h)+\frac{1}{(1-p)}\frac{\partial(q_s B_d)}{\partial x}=0 \tag{21}$$

where $\frac{\partial B_h}{\partial t}hdx=\frac{\partial(B_h h)}{\partial t}-\frac{\partial h}{\partial t}B_h$ and $\frac{\partial Z_b}{\partial t}B_h=-\frac{\partial h}{\partial t}B_h$ have been substituted.

Integration of Eq. (21) with respect to x over the channel length L reads:

$$-\frac{\partial}{\partial t}\int_L B_h h dx+\int_L \frac{1}{(1-p)}\frac{\partial(q_s B_d)}{\partial x}dx=0 \tag{22}$$

where $\int_L \frac{\partial}{\partial t}(B_h h)dx=\frac{\partial}{\partial t}\int_L B_h h dx$ has been substituted, assuming that within a computational time step the increase of the channel length L is negligibly small compared to the increase of the channel cross-sectional area (Bhh).

We define a channel width:

$$B_v=\frac{\int_L B_h h dx}{\int_L h dx}=\frac{V_c}{\int_L h dx} \tag{23}$$

where Vc is the channel volume, Bv is a volume-averaged (or volumetric) width, which is used from now on as a representative width in describing the rate of lateral channel growth. Bv generally approximates Bh and equals Bh in case of uniform prismatic channels.

Insertion of Eq. (23) into Eq. (22) and dividing the equation with the channel length L yields the following general equation of channel growth:

$$\frac{\partial B_v}{\partial t}\frac{\int_L h dx}{L}-\frac{\int_L \frac{\partial Z_b}{\partial t}dx}{L}B_v=\frac{\frac{1}{(1-p)}\int_L \frac{\partial(q_s B_d)}{\partial x}dx}{L} \tag{24}$$

Equation (24) can be transformed into a more compact form by defining other new channel quantities as follows:

$$\frac{\partial B_v}{\partial t}h_L-\left(\frac{\partial Z_b}{\partial t}\right)_L B_v=\left(\frac{\partial A}{\partial t}\right)_L \tag{25}$$

where h_L, $\left(\frac{\partial Z_b}{\partial t}\right)_L$, and $\left(\frac{\partial A}{\partial t}\right)_L$ are the averaged quantities of the channel depth, the vertical growth rate, and the rate of change in cross-sectional area caused by erosion, respectively. They are defined as follows:

$$h_L = \frac{1}{L}\int_L h dx \tag{26}$$

$$\left(\frac{\partial Z_b}{\partial t}\right)_L = \frac{1}{L}\int_L \frac{\partial Z_b}{\partial t} dx \tag{27}$$

$$\left(\frac{\partial A}{\partial t}\right)_L = \frac{1}{L}\frac{1}{(1-p)}\int_L \frac{\partial (q_s B_d)}{\partial x} dx \tag{28}$$

It is noted that Eq. (24) or (25) is of the same form as Eq. (19) but now integrated over the whole channel.

3.3 Relationship between the vertical and lateral growth rates

Definition of the channel cross-sectional growth index

Providing that the instantaneous unit transport rate *qs* is known at any computational section along the channel, Eq. (25) or (19) each still contain two unknown variables i.e. the channel growth rates in vertical and lateral directions. An additional equation is required to be resolved, which is available if we assume a relation between these two growth rates. Therefore, we introduce the channel growth index, which is defined as the ratio of the vertical to lateral growth rate as follows:

$$K_{vl} = \frac{-\left(\frac{\partial Z_b}{\partial t}\right)_L}{\frac{\partial B_v}{\partial t}} \tag{29}$$

where *Kvl* is the channel cross-sectional growth index (sometimes addressed as the growth index hereinafter for simplicity).

Eq. (29) is valid for erosional channels only, i.e. as a whole $\left(\frac{\partial Z_b}{\partial t}\right)_L$ is always negative and $\frac{\partial B_v}{\partial t}$ is always positive.

Visser (1998) implicitly assumes a constant value of *Kvl* throughout the breach erosion process as can be deduced from Eq. (16):

$$K_{vl} = \frac{-\frac{\partial Z_b}{\partial t}}{\frac{\partial B_h}{\partial t}} = \tan\gamma_1 \tag{30}$$

The analytical model by Kraus (2003) suggests a dependency of *Kvl* on both the instantaneous and equilibrium channel geometries (width and depth), and on the constant maximum transport rates through the breach (see Eqs. (17) and (18)).

$$K_{vl} = \frac{h}{B}\frac{Q_{b,\ \max}}{Q_{s,\ \max}}(1-\frac{h}{h_e})/(1-\frac{B}{B_e}) \tag{31}$$

Formulation of the cross-sectional growth index K_{vl}

Tuan *et al.* (2007) carried out a mobile-bed overwash experiment in which the time-dependent morphological development of overwash channels was measured in detail. Table 1 shows the result of the cross-sectional growth index measured from the experiment. It is noted that significant variations of K_{vl} amongst tests and also within runs of one test are observed. Therefore, a constant growth index as determined by Eq. (30) seems doubtful since the channel cross-section changes its form noticeably during different stages of the breaching process. Although Eq. (31) can account for such variation, it is also inappropriate because additional unknown quantities need to be estimated empirically. However, Eq. (31) hints that K_{vl} could be a function of the instantaneous channel geometry and characteristics of the sediment transport through the channel. Hence, we adopt this suggestion and presume that K_{vl} is a function of time.

Table 1 Measured geometry of overwash channels and determination of the growth index

Test	Run	$\overline{\tan\beta}$	$\overline{\tan\gamma}$	K_β	K_γ	B_v	$\bar{B}_v$	h_L	$\bar{h}_L$	$\bar{h}_L / \bar{B}_v$	K_{vl} computed with n =				K_{vl} measured
		(-)	(-)	(-)	(-)	(m)	(m)	(m)	(m)	(-)	1.50	1.65	1.73	2.00	
	t = 0’					0.050		0.010			z	(18)	(19)	(20)	
OW1	t = 10’	0.14	0.56	0.78	0.39	0.242	0.146	0.066	0.038	0.260	0.17	0.30	0.37	0.60	0.34
	t = 20’	0.09	0.54	0.85	0.46	0.319	0.281	0.112	0.089	0.317	0.33	0.55	0.67	1.06	0.71
	t = 0’					0.050		0.010							
	t = 20’	0.17	0.56	0.72	0.39	0.188	0.119	0.038	0.024	0.202	0.11	0.19	0.24	0.39	0.28
OW2	t = 30’	0.15	0.56	0.74	0.39	0.198	0.193	0.040	0.039	0.202	0.11	0.20	0.24	0.39	0.16
	t = 45’	0.14	0.55	0.76	0.42	0.277	0.238	0.064	0.052	0.219	0.14	0.24	0.29	0.47	0.30
	t = 0’					0.050		0.010							
	t = 15’	0.16	0.55	0.73	0.42	0.298	0.174	0.051	0.031	0.175	0.01	0.17	0.20	0.33	0.21
OW3	t = 25’	0.13	0.48	0.79	0.59	0.334	0.316	0.066	0.059	0.185	0.18	0.28	0.33	0.50	0.40
	t = 37’	0.12	0.36	0.80	0.78	0.362	0.348	0.108	0.087	0.250	0.91	1.26	1.45	2.09	1.49
	t = 0’					0.050		0.010							
	t = 16’	0.16	0.55	0.73	0.42	0.265	0.158	0.055	0.033	0.206	0.13	0.22	0.26	0.42	0.26
OW4	t = 30’	0.12	0.55	0.80	0.42	0.334	0.300	0.083	0.069	0.230	0.15	0.26	0.32	0.51	0.41
	t = 39.5’	0.09	0.56	0.85	0.39	0.407	0.371	0.098	0.091	0.244	0.16	0.27	0.33	0.54	0.21

If one assumes that the vertical and lateral growth rates originate from the net transport rates along the bottom and the sides of the channel, respectively, then Eq. (24) can be split up into two separate equations:

$$-\left(\frac{\partial Z_b}{\partial t}\right)_L B_v = \frac{\frac{1}{(1-p)}\int_L \frac{\partial Q_{s,b}}{\partial x} dx}{L} \tag{32a}$$

$$\frac{\partial B_v}{\partial t} h_L = \frac{\frac{1}{(1-p)}\int_L \frac{\partial Q_{s,s}}{\partial x} dx}{L} \tag{32b}$$

in which *Qs,b* and *Qs,s* are instantaneous space-varying total transport rates along the bottom and the sides of the channel, respectively.

To avoid confusion, it should be noted that the lower-case *q* denotes the transport rate per a unit width while the upper-case *Q* is that already multiplied by a width through which sediment is transported.

The separation resulting in Eq. (32) is only meaningful in elaborating the growth index. To predict the channel development Eq. (24) is still required since the transport rate through the channel is always determined as a whole (including the transports both on the bottom and the sides).

The cross-sectional growth index can now be deduced from Eqs. (32a) and (32b):

$$K_{vl} = \frac{h_L}{B_v} \frac{\int_L \frac{\partial Q_{s,b}}{\partial x} dx}{\int_L \frac{\partial Q_{s,s}}{\partial x} dx} = \frac{h_L}{B_v} \frac{Q_{s,bL} - Q_{s,b0}}{Q_{s,sL} - Q_{s,s0}} \tag{33}$$

where notations with subscripts (*0*) and (*L*) denote values at the beginning and end of the channel, respectively.

It is assumed that the pre-entrained sediment content (before entering the channel) is negligibly small compared to the transport in the channel. Also, it is shown in Visser (1998) that the largest transport rate is likely to occur at the end of erosional channels (if the sediment adaptation length is larger than the channel length, which is always the case for Dutch dikes). Therefore, Eq. (33) can be redefined as below:

$$K_{vl} \cong \frac{h_L}{B_v} \frac{Q_{s,bL}}{Q_{s,sL}} = \frac{h_L}{B_v} \frac{Q_{s,b\max}}{Q_{s,s\max}} \tag{34}$$

in which Qs,b_{max} and Qs,s_{max} are instantaneous maximum total transport rates along the bottom and sides of the channel, respectively.

The term $\frac{Q_{s,b\max}}{Q_{s,s\max}}$ in Eq. (34), and so *Kvl*, generally expresses the ratio of sediment transport potential between that on the bottom and on the sides concurrently induced by a flow. Therefore, the determination of the growth index *Kvl* comes down to investigating this ratio in terms of transport capacity.

Considering the total transport load the bed shear stress and the initiation of motion are the major factors that determine the transport capacities along the bottom and along the sides. To develop an expression for the growth index, the total transport rate *qs* is determined following a general power-law form (see Nielsen, 1992, Sections 2.3, 2.4):

$$q_s = M(\tau_b - \tau_{b,c})^n \tag{35}$$

where *n* is a dimensionless transport exponent of the order of 1.5, *M* is a dimensional transport coefficient, τb and $\tau b,c$ are bed shear stress and critical bed shear stress, respectively.

$$\tau_b = \rho g h I \approx \rho g h \tan\beta \tag{36}$$

$$\tau_{b,cr} = \theta_{cr} \rho g (s-1) d_{50} \tag{37}$$

in which *h* is a water depth, θcr is a critical Shields parameter, *I* is the surface gradient which approaches the bed slope $\tan\beta$ at the end of the channel, *d50* is the median diameter of sediment, *s* is the sediment specific density.

Assuming conservation of the net sediment transport volume between the trapezoidal cross-section (bottom width *b*, side slope $\tan\gamma$, and depth *h*) and the equivalent rectangular cross-section (representative width *Bv*, and depth *h*), the sum of the transport rates along the bottom and sides of the channel reads:

$$Q_B = Q_s + Q_b \tag{38}$$

where *Qs, Qb,* and *QB* are the transport rates along the sides, the bottom channel width *b*, and the representative width *Bv*, respectively.

From Eq. (36) and assuming a linear distribution of the bed shear stress from the water surface ($z = hL$) to the bottom ($z = 0$), the shear stress at an arbitrary level *z* above the bed reads:

$$\tau_b = \rho g (h_L - z) \tan\beta \tag{39}$$

To facilitate the elaboration we use intermediary variables so that the critical bed shear stresses (in Eq. (35)) at the sides of the channel can be expressed also through Eq. (39). Equalizing between Eq. (39) and Eq. (37) we derive the following nominal parameters:

$$Z_{cr,b} = h_L - k_\beta \theta_{cr,0} (s-1) d_{50} / \tan\beta \tag{40a}$$

$$Z_{cr,s} = h_L - k_\beta k_\gamma \theta_{cr,0} (s-1) d_{50} / \tan\beta \tag{40b}$$

in which *Zcr,b* and *Zcr,s* are nominal critical heights determined according to the critical bed shear stresses at the bottom and at the sides, respectively, $k\beta$ and $k\gamma$ are factors accounting for effects of the longitudinal (β) and transverse (γ) slopes on the critical Shields parameter, respectively, and $\theta cr,0$ is the critical Shields parameter on a horizontal bed (see Van Rijn, 1993).

$$k_\beta = \frac{\sin(\phi - \beta)}{\sin\phi} \tag{41a}$$

$$k_\gamma = \cos\gamma \left(1 - \frac{\tan^2\gamma}{\tan^2\phi}\right)^{0.5} \tag{41b}$$

with γ is the slope angle of the sides, ϕ is sediment angle of repose.

Using Eqs. 35 and 40, the total transport rate *QB* through the channel with the representative width *Bv* and the depth *hL* is:

$$Q_B = M\left(\rho g h_L \tan\beta - \rho g (h_L - Z_{cr,b}) \tan\beta\right)^n B_v = M(\rho g \tan\beta Z_{cr,b})^n B_v \tag{42}$$

Similarly, the transport rate along the two sides of the channel *Qs* is as follows:

$$\begin{aligned} Q_s &= 2M \int_0^{h_L} \left(\rho g (h_L - z) \tan\beta - \rho g (h_L - Z_{cr,s}) \tan\beta\right)^n \frac{dz}{\sin\gamma} \\ &= 2M(\rho g \tan\beta)^n \frac{1}{\sin\gamma} \int_0^{Z_{cr,s}} (Z_{cr,s} - z)^n dz \end{aligned}$$

$$Q_s = \frac{2M}{n+1}(\rho g \tan\beta)^n \frac{1}{\sin\gamma} Z_{cr,s}^{n+1} \tag{43}$$

The ratio of the transport potential of the bottom to the sides $Q_{s,b} / Q_{s,s}$ reads:

$$\frac{Q_{s,b}}{\mathrm{Q_{s,s}}} = \frac{(Q_b / b) \times B_v}{\dfrac{Q_s}{(2h_L / \sin\gamma)} \times 2h_L} = \frac{B_v}{b} \frac{(Q_B - Q_s)}{Q_s \sin\gamma} \tag{44}$$

in which the relation $Q_b = Q_B - Q_s$ according to Eq. (38) has been substituted.

Insertion of Eqs. (42) and (43) into Eq. (44) and taking $b \approx B_v - h_L / \tan\gamma$ yields:

$$\frac{Q_{s,b}}{\mathrm{Q_{s,s}}} = \frac{1}{2}[(n+1)\frac{B_v}{Z_{cr,s}}\left(\frac{Z_{cr,0}}{Z_{cr,s}}\right)^n - \frac{2}{\sin\gamma}]\frac{B_v}{B_v - h_L / \tan\gamma} \tag{45}$$

It follows from substitution of Eq. (45) into Eq. (34) that:

$$K_{vl} \cong \frac{h_L}{B_v} \times \frac{Q_{s,b}}{\mathrm{Q_{s,s}}} = [(n+1)\frac{B_v}{Z_{cr,s}}\left(\frac{Z_{cr,0}}{Z_{cr,s}}\right)^n - \frac{2}{\sin\gamma}]\frac{h_L}{B_v - h_L / \tan\gamma} \tag{46}$$

Alternatively, we can express *Kvl* by the following equation:

$$K_{vl} = a_1[(n+1)\frac{B_v}{Z_{cr,s}}\left(\frac{Z_{cr,0}}{Z_{cr,s}}\right)^n - \frac{2}{\sin\gamma}]\frac{h_L}{B_v - h_L / \tan\gamma} + a_2 \tag{47}$$

where *a1* and *a2* are dimensionless coefficients to be justified.

By definition, the coefficient *a1* should be in the order of unity ($a_1 = 1$). Mathematically, a_2 can be determined based on a known state. In the present study, channel growth induced by a flow (breach or overwash) starts with an initial (pilot) channel. Hence, the coefficient *a2* can somehow be connected to this initial state of channel growth. In an overflow situation at the very beginning the flow width is always much wider then the flow depth, viz. the initial channel is very flat, so *Bv0 >> hL0,* $\sin\gamma \approx 1$, and *Zcr,s = Zcr,0 = hL0.* Moreover, by the nature of the flow the growth index has a monotonous increase in the early periods (see Table 1). Therefore, it is plausible to assume that *Kvl* ≈ 0 (no cross-sectional growth) at the

start of the process. From these arguments, it can be deduced from Eq. (47) that $a_2 \cong -(n+1)$. It is shown later in the calibration of the index that the above values for the coefficients *a1* and *a2* are appropriate, supporting the nature of the growth index.

Calibration of the growth index

In the following we use existing laboratory data of the channel morphological development to calibrate the two coefficients in Eq. (47). Selection of a suitable value of the transport exponent *n* for two specific cases of erosional channel in the present study, i.e. overwash and breach channels, is also discussed.

The high resolution 3D topographic data of the channel development during overwash tests (see Tuan *et al.*, 2007) allow for an accurate measurement of the growth index according to Eqs. (23), (27), and (29) (see also Table 1). Regression analysis for Eq. (47) using the experimental data of K_{vl} with some common values of the transport exponent n = 1.50, 1.65, 1.73, and 2.0 (1.73 corresponds to the best fit) indicates that a_1 = 1.0 and $a_2 = -(n+1)$ are indeed theoretically appropriate. The comparison of the calculated growth index with that measured in the overwash experiment is shown in Fig. 3.

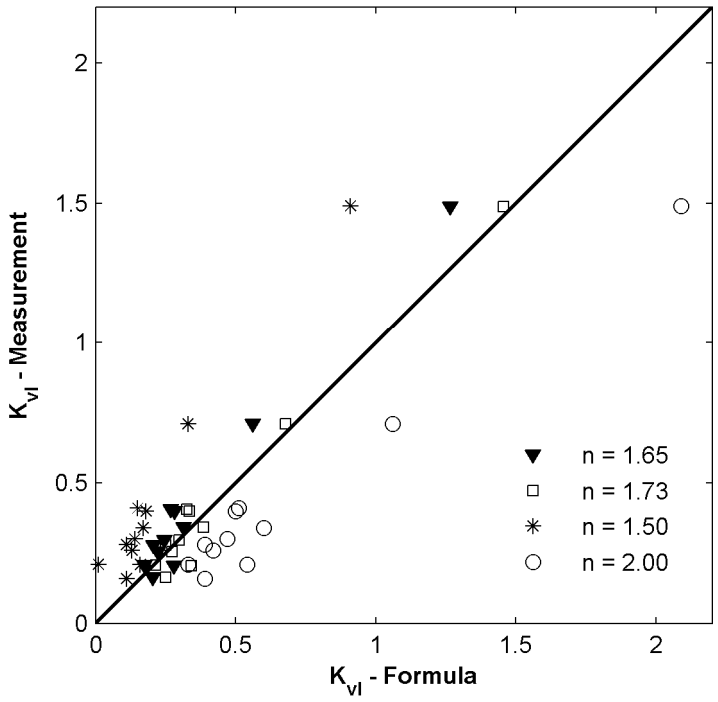

Figure 3 Growth index for overwash channels: measured versus calculated

Using a_1 = 1.0 and $a_2 = -(n+1)$ Eq. (47) becomes:

$$K_{vl} = [(n+1)\frac{B_v}{Z_{cr,s}}\left(\frac{Z_{cr,0}}{Z_{cr,s}}\right)^n - \frac{2}{\sin\gamma}]\frac{h_L}{B_v - h_L/\tan\gamma} - (n+1) \qquad (48)$$

In steep bed channels where $Zcr,0 \approx Zcr,s \approx hL$ (see Eqs. (40a) and (40b)), Eq. (48) reduces further to:

$$K_{vl} = [(n+1)\frac{B_v}{h_L} - \frac{2}{\sin\gamma}]\frac{h_L}{B_v - h_L/\tan\gamma} - (n+1) = \frac{1}{\frac{B_v}{h_L}\tan\gamma - 1}\left((n+1) - \frac{2}{\cos\gamma}\right) \quad (49)$$

It is worth mentioning that the transport exponent *n* in Eq. (48) or (49) is an empirical constant, whose value has been used variously amongst transport formulae (see e.g. Meyer-Peter and Muller, 1948; Nielsen, 1992; Ribberink, 1998). Therefore, it is logical to consider also this exponent in the calibration of the channel growth index.

To investigate the validity of the above finding for overwash channels to the case of breach channels, the laboratory dike breach data of Caan (1996), originally aimed for validation of the BRES model (Visser, 1998), are utilized. In this experiment, bed scour development was unrealistically vigorous during the last period due to scale and model effects (see discussion in Section 4.1). Hence, only part of the experimental data (say up to t = 322 s) is considered realistic and valid for the present purpose. Also, the breach development during the first three stages (up to the breach time t = 135 s; see Visser, 1998) is disregarded since no measurement of the lateral breach growth was conducted for this period. The data for the selected breaching period are given in Table 2. It is worth mentioning that the top width B_t shown in Table 2 was measured at a single section on the dike crest and is not the representative channel width we need. Also, there was no 3D topographic measurement of the breach development in detail. To resolve this, a reasonable approximation of the representative width is given below:

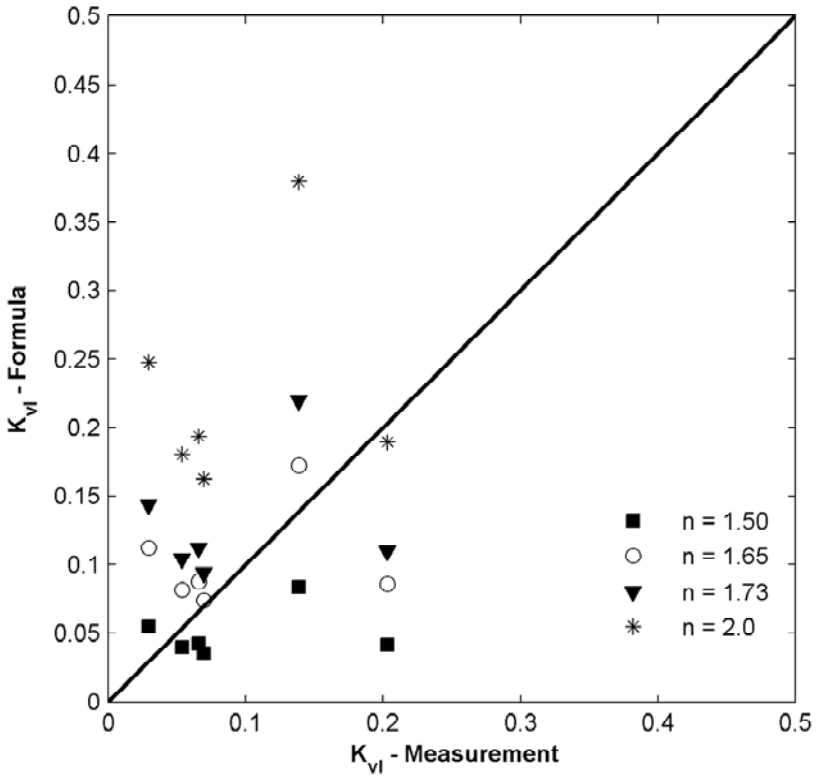

Figure 4 Growth index for breach channels: measured versus calculated

$$B_v = B_t - \frac{h_L}{\tan\gamma} \quad (50)$$

where *Bt* is the top width of the breach channel with a trapezoidal cross-section, the side slope angle $\gamma = 32^o$ (according to Visser, 1998).

Following the same procedure as is done previously for the overwash channels, the determination of the growth index (measured and calculated) for the breaching case is summarized in Table 2. It follows that the calculated values show a monotonous decay over time of the growth index whilst this tendency is not clear from the measurements. This can partly be explained by the uncertainty in the breach data due to small-scale and model effects as addressed in Section 4.1. However, good agreement between the prediction and the experimental data is found for the averaged values over the considered breach period (relative short period of 200 s) of the growth index, particularly for $n = 1.65$. Figure 4 describes the effect of the transport exponent on the accuracy of the prediction for the growth index, which also shows that a reasonable agreement can be achieved with $n = 1.65$.

Table 2 The growth index determined according to the breach data of Caan (1996)

Breach time (sec.)	B_t (m)	h_L (m)	B_v (m)	Calculated K_{vl} with exponents n				K_{vl} Measured
				1.5	1.65	1.73	2.0	
0	0.200	0.030	0.200					
121	0.260	0.073	0.260					
221	0.700	0.109	0.525	0.084	0.172	0.220	0.379	0.1386
242	0.960	0.117	0.773	0.055	0.113	0.144	0.248	0.0295
258	1.090	0.124	0.891	0.043	0.088	0.112	0.194	0.0658
280	1.200	0.141	0.974	0.042	0.086	0.110	0.189	0.2032
301	1.400	0.151	1.158	0.040	0.082	0.104	0.180	0.0538
322	1.580	0.162	1.320	0.036	0.074	0.094	0.163	0.0694
Averaged				0.050	0.103	0.131	0.226	0.093

Discussion

Regarding the nature of the growth index, $Kvl \geq 0$, by definition, does not mean a channel is eroding everywhere; instead it can be sedimentating locally but is eroded as a whole. Because of this non-negativity property of the growth index in erosional channels, one can deduce from Eq. (49) that:

$$\text{or} \qquad \begin{aligned} \cos\gamma &\geq \frac{2}{n+1} \\ \tan\gamma &\leq \frac{1}{2}\sqrt{(n-1)(n+3)} \end{aligned} \tag{51}$$

The above condition also means Eq. (49) is valid only if $\tan\gamma \leq 0.89$ or $\gamma \leq 41^o$ with $n = 1.65$. Therefore, the formulation of the growth index, viz. Eq. (48) or (49), is generally valid for sand channels since their side slopes are about the natural repose angle of sediment ($\gamma < 35^o$).

Some understanding of the channel morphological development can be drawn from the magnitude as well as the variation of the growth index. Regarding breach growth, Table 2 indicates that the growth index is relatively small and gradually decreasing during the last stages of breaching due to overflow, which corresponds to a low rate of the vertical growth and in contrast, a high rate of the lateral growth in this period. In a qualitative sense, this interpretation of the growth index for the considered breaching case is in agreement with the description of the five-stage breach erosion process by Visser (1998). A somewhat different evolution for overwash channels can be understood from the growth index in this case (see Table 2). During the last period of an overwash event, as the barrier crest gets lower and lower, the

overwash flow tends to be more and more intensive. This contradicts with the breaching case, in which the breach flow tends to neutralize near the end. As a result, overwash channels continue to grow vigorously in both lateral and vertical directions even during the last period of the overwash process (until water starts to overflow the crest).

Interesting implications for the channel growth in general can also be deduced from Eq. (49) in that, apart from the power of transporting sediment (exponent *n*), geometric factors considerably affect how the channel grows, e.g. a flatter cross-section (large *Bv/hL*) tends to have a stronger lateral growth and vice versa. Equally, a cross-section of steeper side slopes (a larger $\tan\gamma$ makes smaller $\cos\gamma$) also slows down the vertical growth as can be explained physically by bank avalanching feeding extra sediment into the flow.

The growth index has been calibrated with small-scale experimental data only. The used data are not complete and contain unavoidable uncertainties due to scale and model effects especially in the existing laboratory breach data. Quantitative data from large-scale experiments of the channel growth are therefore desirable to further calibrate the index, to increase understanding of processes involved, and to validate the various model components. Experiments for this purpose should be developed so that the time-dependent channel growth in both vertical and lateral directions and the associated hydrodynamics can be measured in detail.

Numerical discretization and computational procedure

The channel growth equations (Eqs. (19) and (25)) together with the expressions for the growth index derived so far (Eqs. (29) and (48) or (49)) enclose a system of equations which can be solved to describe the time-dependent channel morphological development.

Substitution of Eq. (29) into Eq. (25) yields the following equation describing the increase of channel width *Bv*:

$$\left(h_L + K_{vl} B_v\right) \frac{\partial B_v}{\partial t} = \left(\frac{\partial A}{\partial t}\right)_L \tag{52}$$

Because it is assumed that the net transport volume of sediment is conserved between two cross-sections (see Eq. (38)), the time-dependent increase in the cross-sectional area of the channel, i.e. the right hand side of Eq. (52), can be calculated as follows (instead of its original expression by Eq. (28)):

$$\Delta A_L = \frac{\frac{1}{(1-p)} B_v \int_L \frac{\partial q_s}{\partial x} dx}{L} = \frac{1}{(1-p)} \frac{B_v}{L} (q_{s,L} - q_{s,0}) = \frac{1}{(1-p)} \frac{B_v}{L} q_s^* \tag{53}$$

where *qs,0* and *qs,L* are the sediment transport rates per unit width at the beginning and the end of the channel, respectively, $q_s^* = (q_{s,L} - q_{s,0})$ is the net transport rate over the channel.

Equation (52) now can be rewritten as:

$$\left(h_L + K_{vl} B_v\right) \frac{\partial B_v}{\partial t} - \frac{1}{(1-p)} \frac{q_s^*}{L} B_v = 0 \tag{54}$$

Since the growth index *Kvl* is fully determined using Eq. (46) or (47), the above equation is a genuine partial differential equation with respect to the variable *Bv*, which can be solved numerically using an explicit scheme:

$$B_v(t_j+\Delta t)=B_v(t_j)+\frac{\Delta t}{(1-p)}\frac{B_v(t_j)}{h_L(t_j)+K_{vl}(t_j)B_v(t_j)}\frac{q_s^*(t_j)}{L(t_j)} \tag{55}$$

where *tj* is a previous time level, Δt is a computation time step.

To start the computation with Eq. (55), one needs to know the initial dimensions of the channel (*Bv* and *hL* at t = 0).

Updating of the bed level (at *tj* +Δt) at a computed node is done using Eq. (21):

$$-\frac{\partial}{\partial t}(B_h h)+\frac{1}{(1-p)}\frac{\partial(q_s B_d)}{\partial x}=0 \tag{21}$$

where *Bh* and *Bd* can be calculated via the use of the representative width *Bv*:

$$\begin{aligned} B_h &= B_v-\frac{1}{\tan\gamma}(h_L-h)\\ B_d &= B_v-\frac{1}{\tan\gamma}(h_L-d) \end{aligned} \tag{56}$$

A discretized form of Eq. (21) is as follows:

$$\langle B_h h\rangle(x_i,t_j+\Delta t)=\langle B_h h\rangle(x_i,t_j)+\frac{1}{2(1-p)}\frac{\Delta t}{\Delta x}\left(\langle q_s B_d\rangle(x_{i+1},t_j)-\langle q_s B_d\rangle(x_{i-1},t_j)\right) \tag{57}$$

Consequently, the new bed level at a computed node *i* is:

$$Z_b(x_i,t+\Delta t)=Z_b(x_i,t)+h(x_i,t)-h(x_i,t+\Delta t) \tag{58}$$

It is noted that in case that the channel is sufficiently wide *Bd* ≈ *Bh* ≈ *Bv*, then Eq. (21) and so Eq. (57) reduce to the conventional equation of mass conservation for the bed level only (the Exner equation).

$$Z_b(x_i,t_j+\Delta t)=Z_b(x_i,t_j)-\frac{1}{2(1-p)}\frac{\Delta t}{\Delta x}\left(q_s(x_{i+1},t_j)-q_s(x_{i-1},t_j)\right) \tag{59}$$

Equation (59) can be used in cases when only the bed profile is considered. For instance, in the computation of wave overwash if the initial dimensions of a potential channel are not known in advance and the response of the barrier profile needs to be known to assess the barrier breach initiation.

To avoid abrupt transitions of the bed profile, a numerical smoothing procedure is applied to the newly updated nodes in Eqs. (57) and (58) (see e.g. Horikawa, 1988 and Steetzel, 1993):

$$Z_b(x_i,t+\Delta t)=Z_b(x_i,t+\Delta t)+\frac{1}{2}\psi\left[Z_b(x_{i+1},t)-2Z_b(x_i,t)+Z_b(x_{i-1},t)\right] \tag{60}$$

where ψ is a numerical smoothing factor that depends implicitly on the rate of bed level changes. This factor is in the range of 0.01 ~ 0.05 and should be determined from trial computations.

Figure 5 describes the computational flowchart showing the relation between various model components. At a given computational time step, the modeling of channel growth starts with the computation of the flow parameters along the channel, which gives the required hydraulic input to the sediment transport module. The channel width increase and channel bed changes are then updated using the formulations of the MOGEC approach presented earlier. This routine is iterated until the driving overflow ends.

4 Applications

In this Section the MOGEC approach is applied to simulate the overflow-induced channel growth in two typical situations of hydraulic engineering practice, viz. breach growth and overwash development, to verify its capability. Existing experiments of the channel growth of these types are used for comparison. It is worth mentioning that the determination of the sediment transport rate for use in the MOGEC approach is distinct, depending on the specific flow and transport characters in each situation. Particularly, it is shown in Tuan *et al.* (2006b) that the turbulence in a hydraulic jump plays a role in the breach sediment transport, relevant for the modeling of scour formation and development in the first stages of the breaching process. Hence, local refinements in terms of modeling of flow and transport are necessary for this purpose. Because of their relevance, some of these concerning aspects are also addressed briefly.

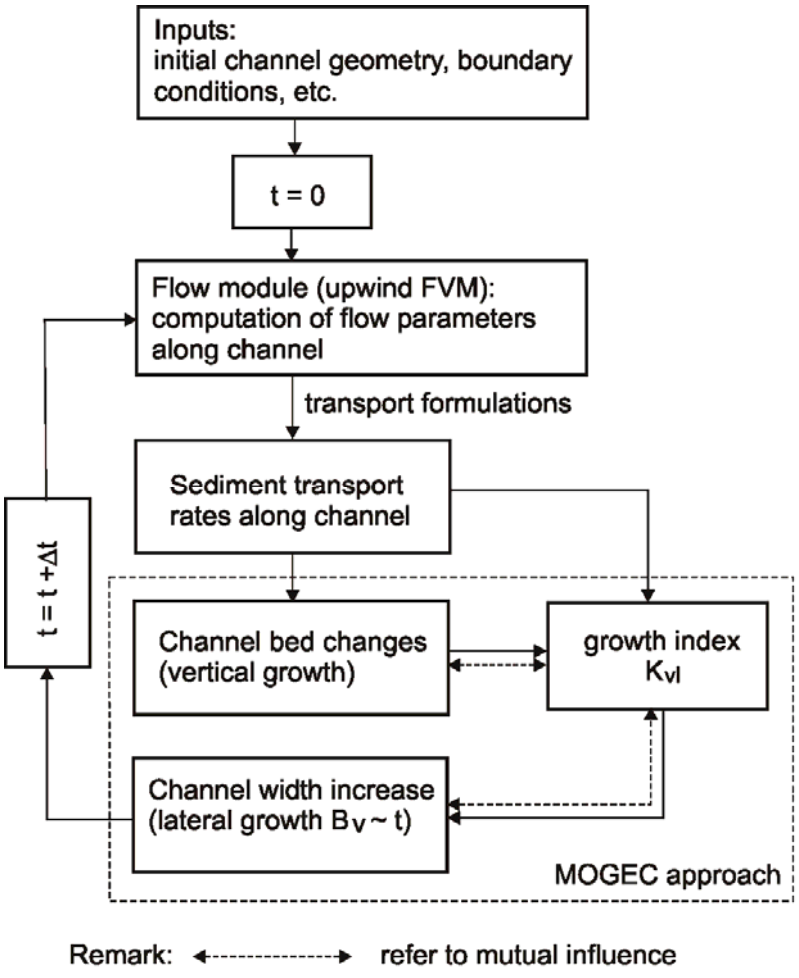

Figure 5 Computational flowchart of channel growth

4.1 Breach growth in a sand barrier

Existing breach experiments

We utilize the data from the existing breach experiments, which were used to calibrate and validate the BRES model of Visser (1998). These include the Zwin'94 field experiment and the laboratory experiment of Caan (1996). In both experiments, the breach was initiated by a small pilot channel made in the crest of the dike. The flow of water through this pilot channel started the breach development process. Details of the experimental procedures and the measurements can be found in Visser (1998) and Caan (1996). In the following only a brief description is given.

The Zwin'94 field experiment was carried out in 1994 in the Zwin channel, a tidal inlet at the Dutch-Belgian border. A sand-dike closing the Zwin channel was built with a height of 2.6 m above the channel bottom and a width at the crest level of 8 m. The pilot channel was 0.8m in depth and width was 1.0 m at the bottom and 3.6 m at the dike crest. The experiment was prepared mainly to capture the breach growth both vertically and laterally. Relevant experimental data on the breach hydrodynamics are very limited since all the velocity measuring stations were located too far away from the main breach stream. Only a few data points of the surface flow velocity measured by floats in the breach are available. Due to a technical failure during the experiment only a limited number of readings of the breach level were logged and only the breach widening at a single location on the dike crest (breach top width) was completely monitored. Because of the incident, the experiment left behind some ambiguity about the scour development and the reliability of the breach bottom level observation. It was then decided to conduct an extra, small-scale laboratory experiment, i.e. Caan's experiment. This dike of 0.15 m high was constructed in a wave basin. Water was pumped into the upper basin section to maintain the upstream water level of the dike as constant as possible. Initially, water flowed through a pilot channel of 3 cm deep and 20 cm wide notched in the dike crest. The flow spilled downstream into a dry sand polder. Video and photo cameras were used to capture the vertical and lateral breach development. The breach profile was video-taped through a glass-wall which acted as the central axis of the breach. Again, data available for calibration of the breach hydrodynamics are limited since this was not aimed in the experiment. It is worth mentioning that questions still remain about the reliability and representation of the quantitative data of morphological breach development in the experiments, especially regarding the vertical breach development. The breach profiles were captured along the glass wall (in the laboratory case) or along the central breach axis (in the field experiment), where the maximum gully depths are expected. Furthermore, there exist uncertainties, e.g. inhomogeneous porosity due to uneven compaction, which cannot be evaluated from the breach data. Appreciable differences in the breach profile evolutions between two control tests with the same hydraulic testing conditions are observed during the laboratory experiment of Caan (1996). This can only be explained by the fact that the sand compaction was different between those tests. Uneven compaction within the dike and its base is also assumed to explain sudden increases of the scour depth in loosely-packed areas as observed in the experiment. The scour depth was sometimes even larger than the mean flow depth and the breach flow resembled a flow pouring into a deep hole. For this reason, the scour depth in the laboratory experiment was in fact dominated by scale and model (geotechnical-related) effects.

In conclusion, quantitative field and experimental data of breach growth in general are so scarce and usually far from complete. Yet, the data from the two existing experiments are still being highly valuable for the present study purpose.

Breach simulations

As already mentioned in Subsection 2.2, an extra source term is added to Eq. (14) to account for the jump turbulence effects in the determination of the jump profile, which is needed for the computation of the flow structure modified by the jump. The source term coefficient $\hat{\beta}$ for the case of breaching reads (see Tuan *et al.*, 2006b):

$$\hat{\beta} = \frac{g\Delta x}{2\hat{c}} \overline{A}(\overline{S}_{bx} - \overline{S}_f + \beta_u S_{jp}) \tag{61}$$

where βu is a nominal relative velocity factor, βu = 2.0 as calibrated with data of existing hydraulic jump experiments (see Tuan *et al.*, 2006b), S_{jp} is the jump head loss slope.

The transport approaches of Van Rijn (1993) and Ribberink (1998) are used for computation of suspended and bed loads respectively. It is referred to Tuan *et al.* (2006b) for details of the computation. Prior to the determination of the bed level changes according to Eqs. (57) through (60), additional smoothing techniques might be required in cases of fast-moving flow to avoid unrealistic sudden changes of the sediment transport rate and thus of the bed level since the flow needs some transitional distance before it can adapt fully to the local conditions (see e.g. Jorgen Fredsoe and Rolf Deigaard, 1992). This is particularly relevant to the breach modeling (see Visser, 1998). Hence, the calculated transport field is smoothed using a response function before it is used in Eq. (57) to update the breach bed level changes:

$$\frac{dq_{st}}{dx} = \frac{q_{st,c} - q_{st}}{L_a} \tag{62}$$

where *qst,c* is the total sediment transport rate obtained directly from the transport module, *qst* is the transport after smoothing and is used for updating the bed changes, *La* is an adaptation length for sediment entrainment.

Visser (1998) indicates that the adaptation length for sediment entrainment plays a role in the breach transport modeling, necessary to compute the breach erosion rate more properly. The author adopted the approach of Galappatti (1983) for *La* to the breaching case as follows:

$$L_a = \xi \frac{ud}{w_s \cos\beta} \tag{63}$$

where *u* is the local fluid velocity, w_s is the sediment fall speed, $\xi < 1$ is an empirical constant, β is the local bed slope (here we use $\cos\beta = \cos\gamma \approx 1$).

In principle, a larger ξ and so *La* would result in a milder erosion rate and vice versa. Appropriate values for ξ should be chosen according to the flow regime (Visser, 1998). Here one can use ξ = 0.10 for jump-affected area and ξ = 0.40 otherwise (see Tuan, 2007).

Figures 6 and 7 show the comparisons of the experimental results of the breach growth in the laboratory dike and the Zwin'94 dike with those predicted using the MOGEC approach respectively.

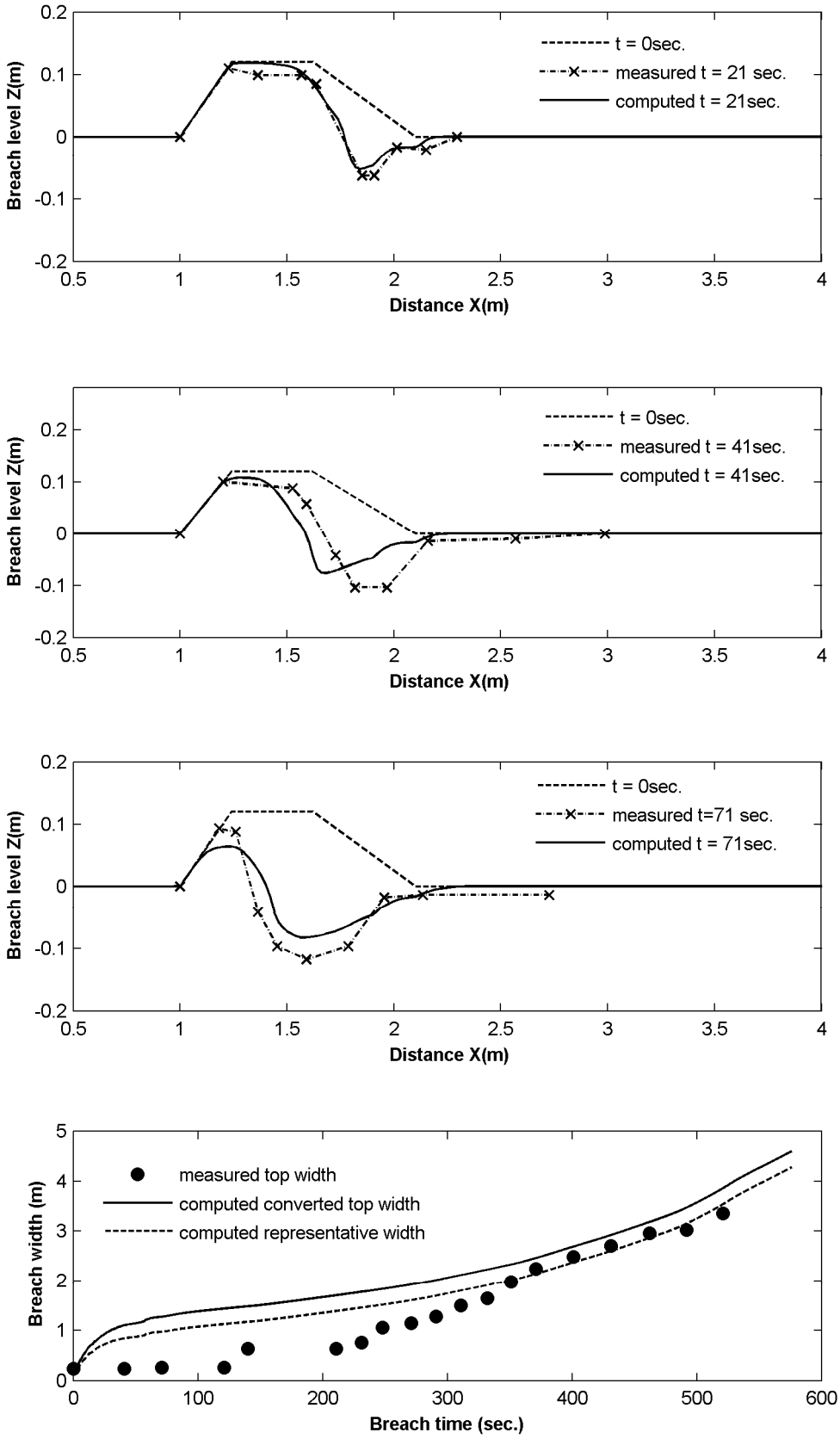

Figure 6 Breach growth in laboratory dike of Caan's (1996)
Upper three graphs: vertical breach growth at various time steps, lower graph: lateral breach growth

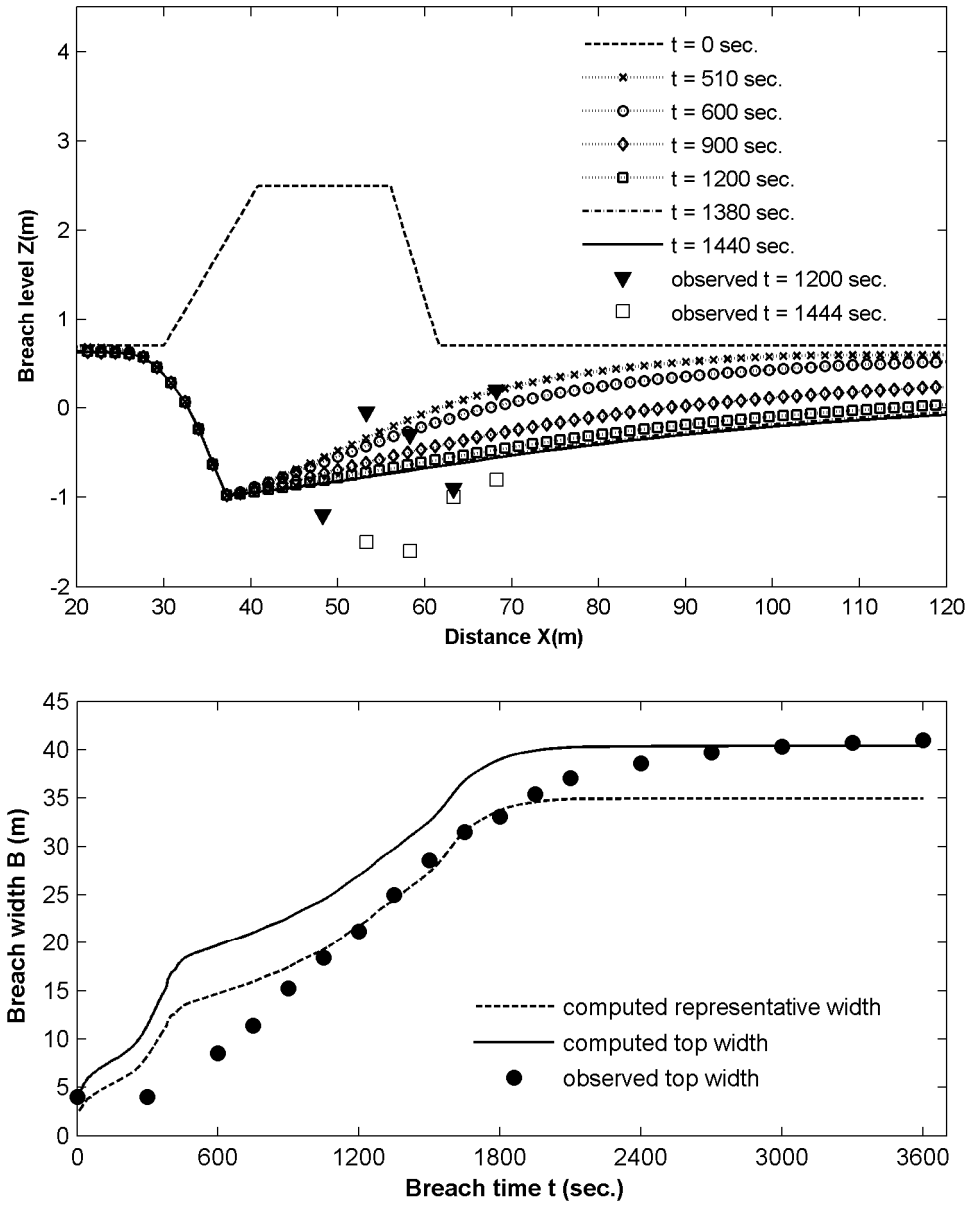

Figure 7 Zwin'94 field dike breach experiment (Visser, 1998)
Upper graph: vertical breach growth at various time steps; Lower graph: lateral breach growth

4.2 Development of overwash channel

Existing overwash experiment

Quantitative data on overwash has been scarce both in laboratory and field conditions. In the present application we use the laboratory overwash data of Tuan *et al.* (2007) that are only one available. The experiment consists of four tests (OW1 to OW4) of model sand barrier of various widths and crest levels constructed in the long wave-sediment flume at Delft University of Technology. Irregular waves of the standard JONSWAP spectra were used in all the tests. Three-dimensional high resolution time-dependent topographic changes of the overwash channel were measured.

Simulation of overwash development

Figure 8 illustrates the response of a low-crested sand barrier during a storm surge, in which wave overwash processes take place on the landward side of the barrier crest. This figure was derived from an overwash test of Tuan's experiments (see Tuan *et al.*, 2007). It is noted that processes of beach and dune erosion on the seaward side taking place simultaneously with wave overwash are not addressed in the present article.

In order to compute the overwash flow and subsequently the morphological development of the overwash channel according to the MOGEC approach, one first needs to quantify the hydraulic input, i.e. wave overtopping parameters, at the entrance boundary to the channel. For this purpose, in most conventional approaches (see e.g. Tega and Kobayashi, 1999) the average overtopping discharge and thickness are used. However, these average quantities are found not to represent the overtopping nature adequately such as its intermittent character and associated strength, making it inappropriate for overwash modeling. To overcome this, Tuan *et al.* (2006a) have formulated the average instantaneous overtopping discharge and thickness according to an event-based approach as functions of the seaward hydraulic and barrier geometric conditions. It is assumed that wave overtopping on the crest of a dike or a barrier resembles a simple boundary layer flow without any strong turbulence-generated mechanism (see Tuan *et al.*, 2006a and 2007). Hence, one just adopts the above numerical approach for modeling of the overwash flow without any extra source term in Eq. (14).

Because of space limitation only the result of test OW4 of the above overwash experiment is shown here in Fig. 9 for comparison. It is referred to Tuan *et al.* (2007) for results of all the tests. In the computation, the transport approaches of Van Rijn (1993) and Ribberink (1998) are selected for determining the overwash sediment transport rate respectively.

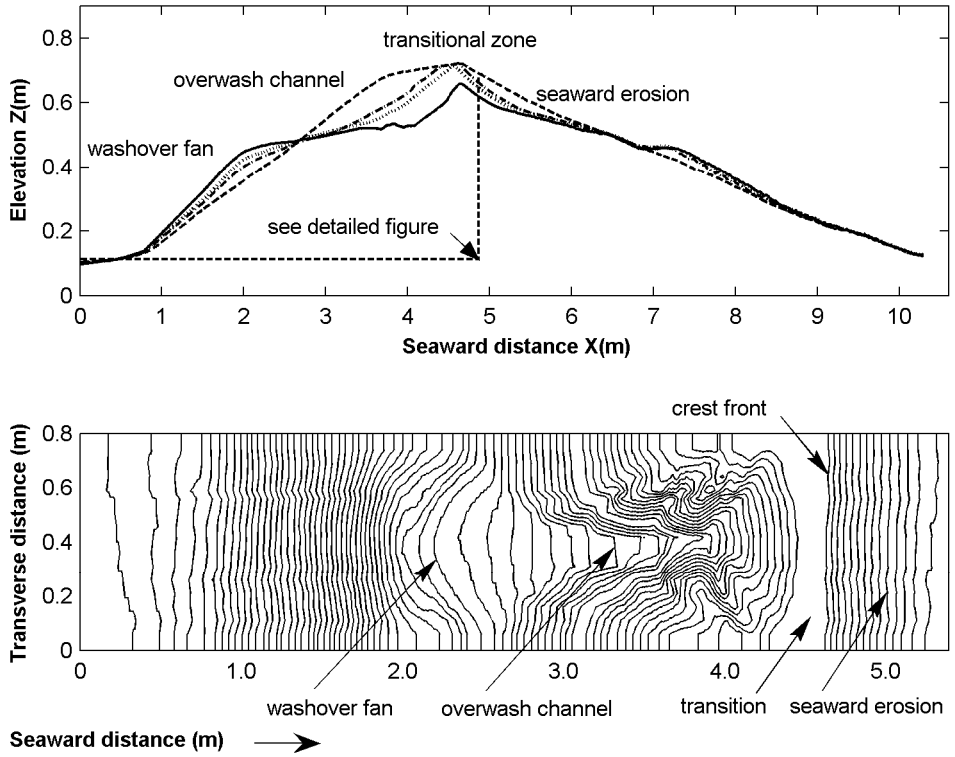

Fig. 8 Barrier response during storm surges showing overwash development on the landward side

4.3 Discussion

As appears from the comparisons between observations and calculations considerable discrepancies are still present especially for the breaching cases. The breach depth is systematically underestimated for situations of both laboratory and field experiments. This can partly be attributed to the uncertainties in the breach data as discussed earlier. More importantly, although the approach allows us to simplify the modeling channel growth considerably, the modeling capability in general still largely depends on the reliability of the sediment transport computation. Most transport formulations are inappropriate outside the laboratory conditions for which they were developed. Our understanding of physical processes involved is still far from complete. As an example, it is shown in Tuan (2007) that more insight into the sediment transport processes under effects of strong turbulence (e.g. induced by a turbulent hydraulic jump) is needed in order to better model the breach growth in sand barriers.

Two other aspects also influence the model predictions. First, the present approach assumes a trapezoidal channel cross-section with uniform side slopes. These slopes, usually taken as the angle of internal friction of the sediment, have effects on the growth tendency of the channel as discussed in Section 3.3. However, the channel cross-section in reality can be more complex having different side slopes above and below the water line (Visser, 1998). The assumption of uniform side slopes might therefore be too simplistic. Second, breach widening due to bank avalanching is an element in modeling the growth of non-cohesive channels. This lateral erosion process is discrete both in time and in space. In the present approach, its effects on the channel growth are implicit through the introduction of the growth index. In an improved process-based approach this would require explicit modeling.

Notwithstanding the discussed limitations, in both considered situations of channel growth, a satisfactory agreement between the computed results using the MOGEC approach and the measurements is found. The approach has proven to be sufficiently reliable and is efficient for use in morphodynamic models, providing ample possibilities for improvement when more detailed experimental results become available.

5 Summary and conclusions

In this paper a new process-based approach for modeling the growth of erosional channels induced by overflow is introduced. The goal is to model this morphological process in a more efficient way, i.e. computationally inexpensive but sufficiently reliable.

The flow modeling is based on the shallow water equations, which can be solved using any robust upwind numerical scheme such as the first-order Riemann approximation by Roe (1981) to resolve numerical difficulties arising from complex flow conditions. For the computation of the channel growth in both vertical and lateral directions, a set of closed equations has been derived in connection with several new morphologic parameters such as the representative channel width and the channel cross-sectional growth index. To this end, it is assumed that the channel expansions in vertical and lateral directions originate from the net sediment transport rates along the bottom and the sides of the channel respectively. The growth index is defined as the ratio of the vertical growth rate to the lateral one and is found to depend mainly on the instantaneous channel geometry and the sediment transport exponent. The parameter has been calibrated with existing experimental data of breach growth and of overwash channel development.

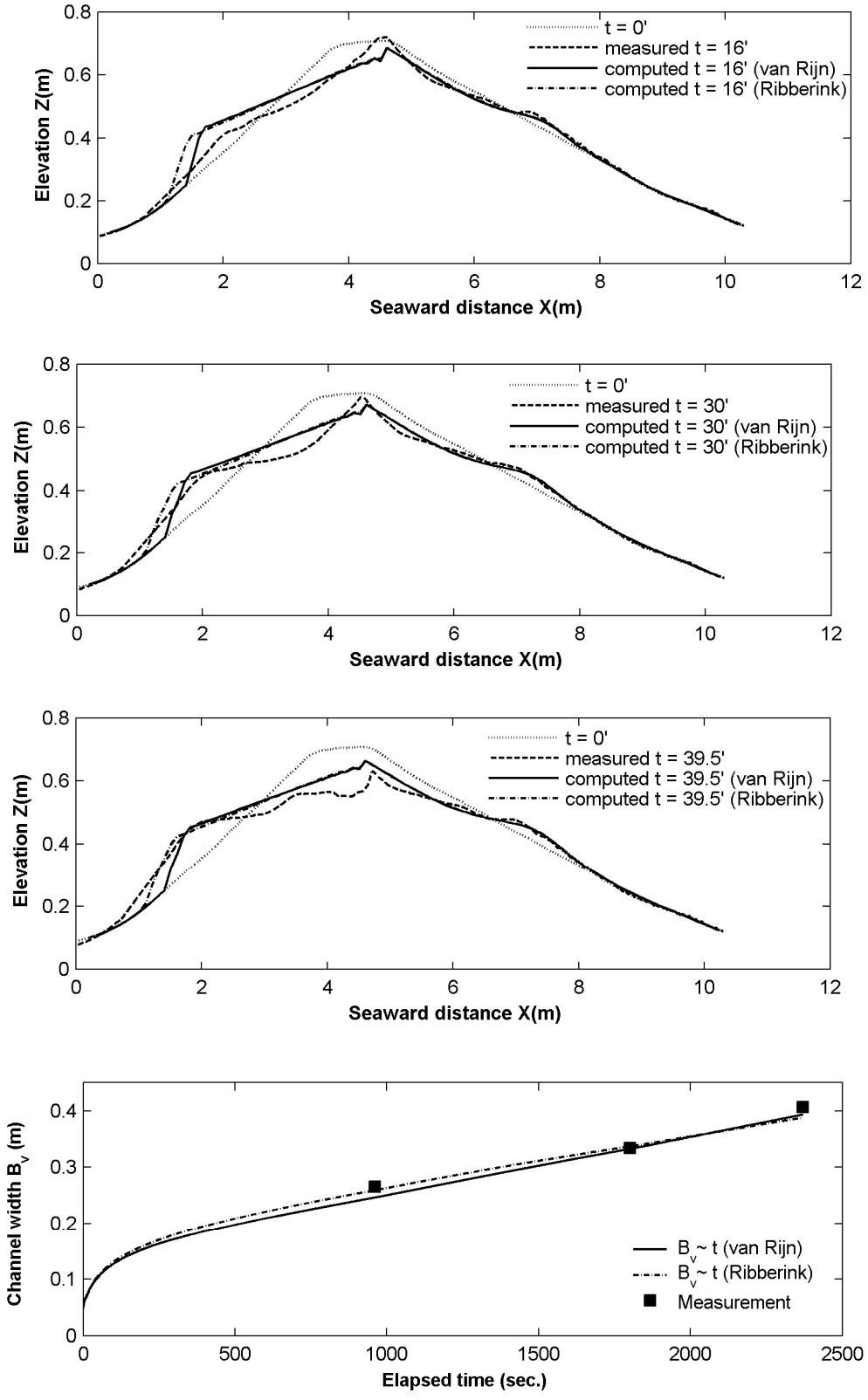

Fig. 9 Barrier response during storm surges: computed versus measured
upper three graphs: barrier profile response at various time steps, lower graph: lateral overwash growth

The developed approach has been applied to simulate the overflow-induced channel growth in two typical situations, i.e. the breach growth in sand dikes and the overwash channel development across sand barriers. Computational results give satisfactory resemblance with existing experimental data.

In conclusion, the new approach allows for an efficient process-based computation of the channel growth in both vertical and lateral directions. The approach appears to be reliable and suitable for incorporating in 1D/2DV morphodynamic models. Implications on the general tendency of channel growth induced by overflow have also been drawn out.

Recommendation for future research includes further verification of the present approach with additional quantitative data of the time-dependent channel growth from large-scale experiments. Large-scale experiments are also needed for better understanding of processes involved with sediment transport, which is crucial for improvement of the capability of modeling of channel growth in general. The present approach is conceptually adaptable to modeling the breach growth of cohesive (clay) dikes. It is therefore recommended to investigate this possibility of adaptation.

Acknowledgements

The authors acknowledge the financial support via the collaborative project in Coastal Engineering between Delft University of Technology and Hanoi Water Resources University.

References

Busnelli, M.M., 2001. Numerical simulation of free surface flows with steep gradients. *Communications on Hydraulic and Geotechnical Engineering*, Rep. No. 01-3, Delft Univ. Techn., Delft, the Netherlands, 180 pp.

Caan, C.P., 1996. Bresgroei: een experimental onderzoek naar de ontwikkeling van de ontgrodingskuil (Breach growth: an experimental investigation of the development of the scour hole), *Master thesis*, Hydraulic and Geotechnical Eng. Div., Dept. Civ. Eng., Delft Univ. Techn., Delft, the Netherlands, 100 pp.

Galappatti, R., 1983. A depth-integrated model for suspended transport. *Communications on Hydraulics*, Rep. No. 83-7, Delft Univ. Techn., Delft, the Netherlands.

Garcia-Navarro, P. and Vazquez-Cendon, M. E., 2000. On numerical treatment of the source terms in the shallow water equations. *Computer & Fluids*, Elsevier, 29, pp. 951-979.

Horikawa, K. (ed.), 1988. Nearshore dynamics and coastal processes: theory, measurement, predictive models. *Univ. Tokyo Press*, 522 pp.

Jorgen Fredsoe and Rolf Deigaard, 1992. Mechanics of coastal sediment transport, *Advanced Series in Ocean Engineering*, *World Scientific*, Singapore, Vol. 3, 369 pp.

Kraus, N.C., 2003. Analytical model of incipient breaching of coastal barriers. *Coastal Engineering Journal*, 45, 4, pp. 511-531.

Mayer-Peter, E. and Muller, R., 1948. Formulas for bed-load transport. *Proc. 2nd Congress IAHR*, Appendix 2, pp. 39-64.

Nielsen, P., 1992. Coastal bottom boundary layers and sediment transport. *World Scientific*, Singapore, 324 pp.

Ribberink, J. S., 1998. Bed-load transport for steady flows and unsteady oscillatory flows. *Coastal Engineering*, 34, pp. 59-82.

Roe, P.L., 1981. Approximate Riemann solvers: parameters and difference schemes. *J. Computational Physics*, 43, pp. 357-372.

Steetzel, H.J., 1993. Cross-shore transport during storm surges. *Delft Hydraulics Communication*, Rep. No. 476, Delft, the Netherlands, 291 pp.

Tega, Y. and Kobayashi, N., 1999. Numerical modeling of over-washed dune profiles. *Coastal Sediment'99, ASCE*, pp. 1355-1369.

Toro, E.F., 1997. Riemann solvers and numerical methods for fluid dynamics: a practical introduction. *Springer-Verlag*, Berlin, 624 pp.

Tuan, T.Q., Verhagen, H.J, Visser, P.J. and Stive, M.J.F., 2006a. Wave overwash at low-crested beach barriers, *Coastal Engineering Journal*, 48, 4, pp. 371-393.

Tuan, T.Q., Verhagen, H.J and Visser, P.J., 2006b. Advances in one-dimensional breach modeling of coastal sand barriers. *Proc. 3rd Int. Scour Erosion Conf.*, Amsterdam, the Netherlands, pp. 649-658.

Tuan, T.Q., Verhagen, H.J., Visser, P.J. and Stive, M.J.F., 2007. Numerical modeling of wave overwash on low-crested sand barriers. *Proc. 30th Coast. Engrg. Conf.*, San Diego, USA, World Scientific Press, pp. 2831-2843.

Tuan. T.Q., 2007. Seasonal Breaching of Coastal Barriers. *Doctoral Dissertation*, Faculty of Civil Engineering and Geosciences, Delft University of Technology, The Netherlands, 192 pp.

Van Rijn, L.C., 1993. Principles of sediment transport in rivers, estuaries and coastal seas. *Aqua Publications*, Amsterdam, the Netherlands.

Visser, P.J., 1998. Breach growth in sand-dikes. *Communication on Hydraulic and Geotechnical Engineering*, Rep. No. 98.1, Delft Univ. Techn., Delft, the Netherlands.